

Cyclic Behavior of Multidirectional Box-Shaped Shearing Damper: Experimental Study

Angga Fajar Setiawan¹, Ali Awaludin^{1*}, Iman Satyarno¹, Noorsuhada Md Nor², Yusuf Haroki¹, M. Fauzi Darmawan¹, Sidiq Purnomo³, Ignatius Harry Sumartono³

¹Department of Civil and Environmental Engineering, Universitas Gadjah Mada, Yogyakarta, INDONESIA

²Centre for Civil Engineering Studies, Universiti Teknologi MARA, Cawangan Pulau Pinang, Kampus Permatang Pauh, Pulau Pinang, MALAYSIA

³PT Wijaya Karya Beton, Jakarta, INDONESIA

*Corresponding author: ali.awaludin@ugm.ac.id

SUBMITTED 8 July 2024 REVISED 23 November 2024 ACCEPTED 19 December 2024

ABSTRACT This paper discusses an experimental study investigating the behavior of the multidirectional box-shaped shearing damper (MBSD) proposed for a bridge structures application. The MBSD consisted of a box-shaped steel plate hot coil (SPHC) material with an effective dimension of $100 \times 100 \text{ mm}^2$ designed to dissipate earthquake excitation energy under the combined resultant forces from the longitudinal and transversal directions. The specimens varied in two different web slendernesses, i.e., 58.8 and 27.0. Furthermore, to investigate the different load direction effects, four different loading angles with respect to one of the web planes, i.e., 0° , 15° , 30° , and 45° to be implemented. The specimens were subjected to cyclic loading according to AISC/ANSI 341-22. In the experiment, the shear yield strength, ultimate state behavior, and energy dissipation achievement were evaluated. The results showed that MBSD could achieve shear strength and sufficient energy dissipation under different angles of loading directions, ranging from yielding to ultimate deformation state. The yielding and ultimate characteristics of MBSD were similar to those of an ordinary shear panel damper. A stockier web resulted in greater stability in stiffness after the yield point and less buckling of the web but also a slightly earlier strength degradation due to earlier fracture damage at the welded joint. Finally, the MBSD device had feasibility for application in bridge structure as a seismic device by considering appropriate strength and deformation capacity compatibility adjustments with the ultimate displacement limit of 0.11 rad drift angle. In addition, a recommendation for using a better elongation capacity steel material and less welding assembly will improve the behavior and seismic performance of the MBSD.

KEYWORDS Cyclic loading, Shear yield strength, Energy dissipation, Loading angles, Ultimate

© The Author(s) 2025. This article is distributed under a Creative Commons Attribution-ShareAlike 4.0 International license.

1 INTRODUCTION

The hysteretic damper device composed of steel material was adopted for use in bridge piers to reduce seismic demand and structural cost (Xiang et al., 2019). One type of hysteretic damper is a shear panel damper (SPD), in which energy dissipation is produced from the shear-yielding mechanism (Nakashima et al., 1994). The SPD was installed in a fused parallel structural system to the pier with multi-columns and worked in one direction of pier's lateral deformation within the frame system's plane (Chen and Usami, 2007; Sun et al., 2004; Nakamura et al., 2014). In other studies (Tetsuhiko, 2011; Tetsuhiko et al., 2010; Haroki et al., 2023; Santoso et al., 2024; Emilidardi et al., 2024), the SPD was installed in series with the pier structure and in parallel with the bearing of the simple support or continuous bridge superstructure. However, using a common SPD with a one-directional configuration provides a huddle configuration of the bearing support with both longitudinal and transverse SPD on the pier head (Awaludin et al., 2022). The circular hollow steel damper (Abebe et al., 2019; Kori Effendi and Yulianto, 2023), finned-tubular multidirectional shear

panel damper (FT-MSPD) (Emilidardi et al., 2022), and cross-web type multidirectional shear panel damper (CW-MSPD) (Utama et al., 2022) have been proposed for use as multidirectional shearing-based seismic devices. Nevertheless, due to their complex shape and configuration, their fabrication process remains challenging. Therefore, other typical configurations of multidirectional shearing damper (MSD) that are easily fabricated need to be developed.

In other studies, using a metal-based square-shaped section hysteretic damper was studied by some researchers. Shirinkam and Razzaghi (2020) studied the box-shaped damper with a bending yielding mechanism under axial loading. Xiao et al. (2022) investigated a shear square section steel tube damper for an in-plane loading-only application. Then, Awaludin et al. (2022) proposed a bidirectional shear panel damper with a square hollow section (MBSD-SHS) for a simply supported bridge using a numerical modeling study. It used a fully square hollow section without any welded connection. However, achieving the appropriate high

elongation steel material specification is challenging when using square hollow sections (SHS). In addition, the study by Awaludin et al. (2022) was only conducted with numerical modeling under monotonic loading in the edge plane without variations in loading angle direction out of the plane of web edges. Meanwhile, in the application of a multidirectional shearing damper for bridge structures, the resultant superstructure seismic motion from the longitudinal and transversal combination could be arbitrary. Thus, it is uncertain whether it will work in the plane of the shearing damper edges. According to the previous studies mentioned above, it was found that no experimental studies have been conducted to determine the performance of multidirectional box-shaped shearing damper (MBSD) with steel plates at different loading angle orientations. Therefore, an experimental study of a shearing damper composed of steel plates under cyclic loading and varying loading angle directions out of the plane of web edges needs to be conducted to examine the device's performance for actual implementation.

This study aimed to investigate the behavior and performance of MBSD for a bridge structure's seismic energy dissipation device. The seismic device consists of a box-shaped steel plate as the shear panel that could achieve yielding under shear deformation at a multidirectional loading angle. The box-shaped steel plate configuration of MBSD is designed for a simple fabrication method. The shear-yielding deformation is expected to achieve sufficient energy dissipation below the ultimate displacement limit. In addition, the box shape could generate larger shear resistance out of the plane on the web edge, which aligns with the resultant seismic load demand on the bridge under the combination of longitudinal and transversal directions. The shearing damper cross-section is configured with four steel plates with welded connections to build the box shape with an effective size of $100 \times 100 \times 100 \text{ mm}^3$. The specimens varied by two different web slenderness and four different loading angles relative to the web direction. In the testing, the specimens were subjected to quasi-static cyclic loading following the AISC/ANSI 341-22 (Seismic Provisions for Structural Steel Buildings). The recorded hysteresis loops were evaluated to capture the backbone curve along with deformation limit state and energy dissipation.

2 MATERIALS AND METHODS

In this study, the process started with the preparation of test specimen of a MBSD. The experimental work was carried out using four loading directions applied to the specimen: 0° , 15° , 30° , and 45° . During the experimental work, cyclic loading was applied. All the data were then analysed and compared to the theoretical formulation.

2.1 MBSD specimens

To determine the behavior of an MBSD, as illustrated in Figure 1 (a), the experimental variables corresponded to the investigation of the slenderness and the direction of the loading angle was determined. For investigating the web's slenderness (ratio of depth to thickness) in relation to the seismic behavior, two variations of the web's slenderness of the MBSD web slenderness were chosen, namely S-58.8 and S-27.0. To examine the effects of the different loading angles, four variations of loading direction, 0° , 15° , 30° , and 45° , were chosen, as illustrated in Figure 1 (b). The specimens were named according to the variations in slenderness ratio and load angle orientation, as presented in Table 1.

For the specimens, the web sections were made of a sheet plate hot coil (SPHC) with yield strength (f_y) is 338 MPa and 258 MPa for S-58.8 and S-27.0, respectively. The base plate was made from mild steel classified as SS400. The configuration of MBSD is shown in Figure 2 (a). Four specimens for the uniaxial test on SPHC steel material were subjected to a uniaxial testing machine following the ASTM E 8-04 (Standard Test Methods for Tension Testing of Metallic Materials). All specimens were then tested under cyclic loading with a linear vertical displacement transducer positioned at a designated location. Details of the SPHC steel material properties for the web plate are shown in Table 2.

2.2 Experimental setup

The loading setup system was adopted by Kurdi et al. (2017). The experimental load setup for this study is shown in Figure 2 (b) and consists of a load beam, bottom support, column support, and bracket. The load beam was attached to a load cell, as shown in Figure 2 (b), to apply the cyclic load to the specimen. The load frame system supported the MBSD specimens with fixed boundary conditions on both the top and bottom using two base plates. Both the upper and lower base plates were connected to the load cell and lower support with some preloaded bolts. The bolt preload force was set for to ensure that the frictional force between the base plate and the load beam was greater than the shear strength of the MBSD specimens, preventing slippage. The bracket was designed as a rolling support to accommodate the frictionless movement of the loading beam relative to the column support.

During the loading process, the specimens' structural responses were monitored with a digital measurement system, as shown in Figure 2. The generated lateral load generated by the actuator was monitored using loadcell. One linear variable displacement transducer (LVDT) was installed to measure the relative displacement of the loading beam with respect to the loading

frame base plate, as shown in Figure 3. A digital data acquisition system was installed to collect measured displacement and force data from both the LVDT and load cell at a 5Hz sampling rate. At the end of each end cycle load, the deformed shape of the specimens was captured with a camera. The proposed MBSD resembled a link element; therefore, the cyclic loading protocol test

adopted the link element according to the AISC/ANSI 314-22 (AISC, 2022) criteria. The cyclic displacement control target was set at a 0.21 rad drift angle, according to the predicted fracture failure state of the steel material, at which the lateral resistance decreased by around 85%, as shown in Figure 4.

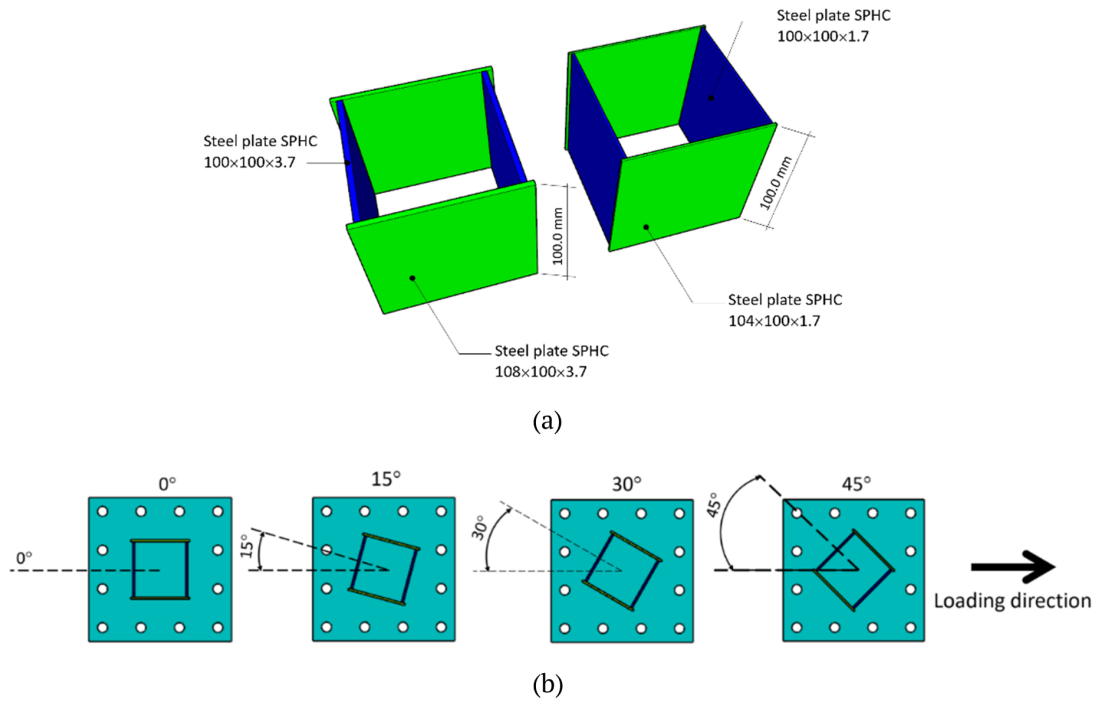


Figure 1 Specimen illustration: (a) detail of MBSD web configuration and (b) loading direction variable.

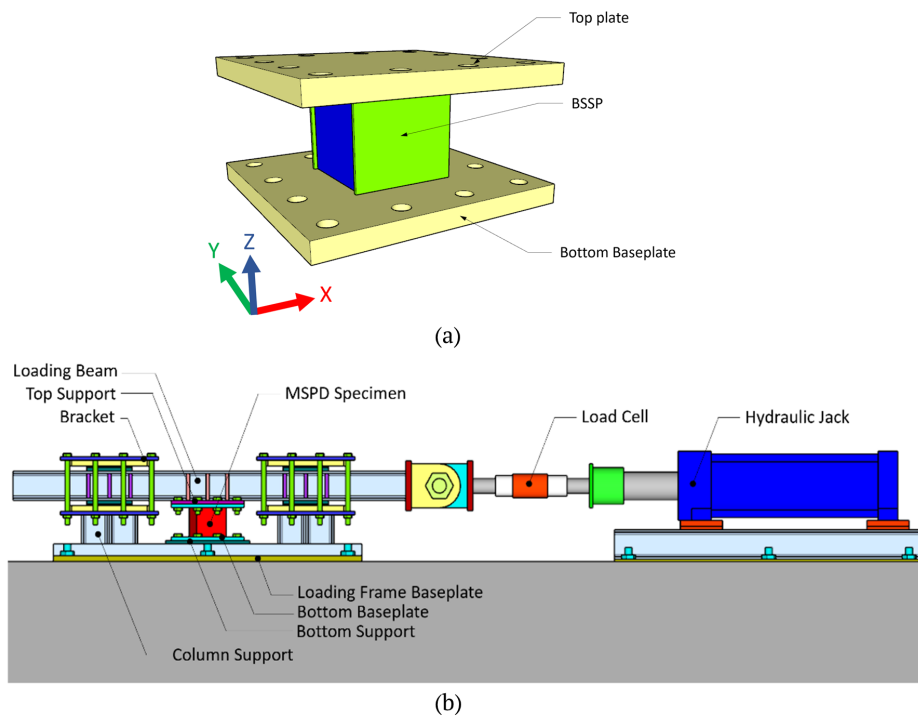


Figure 2 The configurations of (a) the specimen configuration and (b) the overall configuration of the experimental setup.

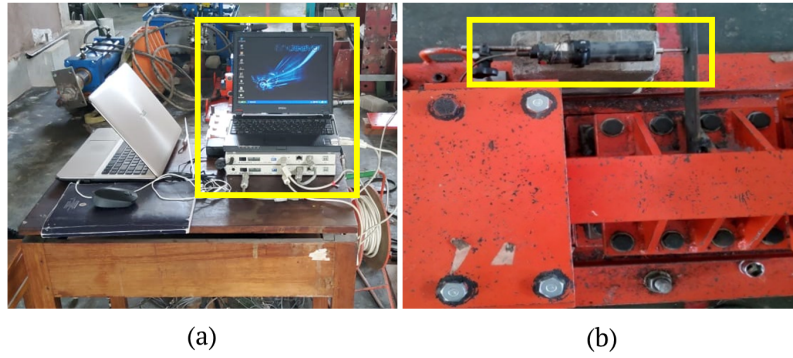


Figure 3 Experimental tools: (a) data acquisition and (b) LVDT.

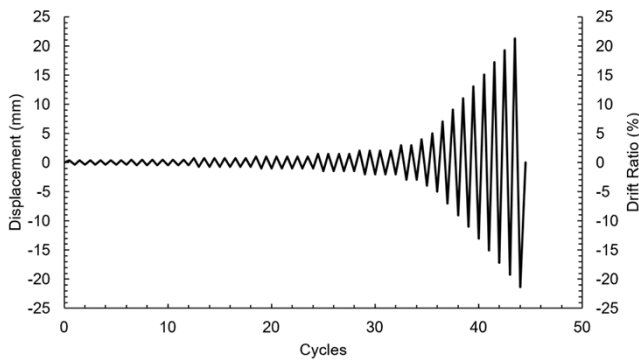


Figure 4 Cyclic loading protocol according to AISC/ANSI 314-22 (Seismic Provisions for Structural Steel Buildings).

2.3 Analytical

In this study, the experimental data of structural response, i.e., force and displacement, were interpreted as a hysteretic curve. Furthermore, the hysteretic curve was used to evaluate the achievement of deformation and shear strength at both yield and ultimate conditions, as well as the energy dissipation achieved.

To analyze shear yield strength, the experimental results were compared with theoretical predictions using an analytical approach. It involved two assumptions regarding the web’s part state: first, initial yield (lower bound) (Awaludin et al., 2022), and second, fully yielding (upper bound) (AISC, 2020) as formulated with Equations (1) and (2), respectively. For inelastic buckling and full plastic deformation of the designed web, the value of C_{v2} was assumed to be 1, as formulated in Equations (3).

To accommodate variations in shear yield strength due to loading angle, both Equations (1) and (2) incorporated the summation of the webs vector resistance, as formulated in Equation (4). V_y and V_{Ry} are the shear yield strength and the resultant shear yield strength of the web, respectively. h , t_w , a , and I are the depth, thickness, height of the webs, and moment of inertia on the shearing cross-section. F_y , τ_y , and E are uniaxial

Table 1. Specimen variations

Name of specimens	Dimension (mm)				$\lambda = h/t_w$	Loading angle orientation
	h	a	w	t_w		
S-58.8-0°	100	100	100	1.7	58.8	0°
S-58.8-15°	100	100	100	1.7	58.8	15°
S-58.8-30°	100	100	100	1.7	58.8	30°
S-58.8-45°	100	100	100	1.7	58.8	45°
S-27.0-0°	100	100	100	3.7	27.0	0°
S-27.0-15°	100	100	100	3.7	27.0	15°
S-27.0-30°	100	100	100	3.7	27.0	30°
S-27.0-45°	100	100	100	3.7	27.0	45°

Table 2. Tensile test properties of SPHC steel material for the web part

Specimens ID	f_y (MPa)	f_u (MPa)	ϵ_u	ϵ_{fr}
SPHC-S-58.8-1	340	428.0	0.170	0.27
SPHC-S-58.8-2	336	427.0	0.160	0.29
Average SPHC-S-58.8	338	427.5	0.165	0.28
SPHC-S-27.0-1	255	389.0	0.150	0.26
SPHC-S-27.0-2	261	354.0	0.170	0.28
Average SPHC-S-27.0	258	371.5	0.160	0.27

yield stress, shear yield stress, and elastic modulus of steel material of the webs, respectively. C_{v2} , k_v , and C_{v1} are the web shear buckling strength coefficient, web elastic buckling coefficient under shear, and the loading angle, respectively. The theoretical shear yield displacement was calculated as the shear yield strength divided by the shear modulus.

Regarding seismic performance assessment parameters, energy dissipation was calculated using the trapezoidal numerical integral method. In addition, the effectiveness of energy dissipation was evaluated by calculating the equivalent viscous damping ratio according to Jacobsen’s theory (Jacobsen, 1930).

$$V_y = \frac{8\tau_y I}{h^2 + \frac{a+2t_w}{2t_w} [(h+2t_w)^2 - h^2]} \cdot C_{v2} \quad (1)$$

$$V_y = 2 \cdot h \cdot t_w \cdot \tau_y \cdot C_{v2} \quad (2)$$

$$\frac{h}{t_2} < 1.10 \sqrt{\frac{k_v E}{F_y}}; C_{v2} = 1 \quad \text{with } k_v = 5 \quad (3)$$

$$v_{Ry} = V_y (\sin \gamma + \cos \gamma) \quad (4)$$

3 RESULTS

3.1 S-58.8 specimens

3.1.1 Hysteresis loop

According to the experimental test of the S-58.8 specimens, the stable hysteresis loop of specimens S-58.8-0° and S-58.8-15° could achieve up to 0.16 rad drift angle with slight pinching, as shown in Figure 5. Figure 6 shows the premature plastic web buckling triggered the pinching hysteresis loop under a 0.02 rad to 0.05 rad drift angle. However, in S-58.8-3° and S-58.8-45°, the hysteresis loop stability could not be maintained after the buckling occurred.

3.1.2 Shear yield strength

Based on the experimental results depicted in Figure 7 (a) and (b), the shear yield strength of the S-58.8 specimens was 51 kN to 58 kN. The general trend, on the raising of the loading angle, the shear yield strengths of each specimen increased with a gradual pattern, as shown in Figure 7 (b). However, the S-58.8-0° generated a slightly larger shear yield strength than S-58.8-15°. The effect of fabrication imperfection might have triggered a larger buckling, reducing the shear resistance. In comparison, as shown in Figure 7 (b), even though the initial shear yield strength (IY) with the analytical approach of specimen S-58.8-0° exhibited a coincident result to the experimental result, there was a sharper increase in trend as the larger the loading angle direction. In addition, the full shear yield strength (FY) of the analytical approach showed a similar trend with a larger magnitude than the initial shear yield strength (IY).

3.1.3 Ultimate state

On average, the ultimate shear strength obtained from experimental results was 1.26 times greater than the shear yield strength, as shown in Figure 7. For all S-58.8 specimens, the ratio of ultimate shear strength to shear yield strength achievement was 1.1 to 1.6. The loading angle effect caused variations in drift angle capacity in the ultimate shear resistance. According to the analytical approach, as shown in Figure 7 (a), the full shear yield strength (FY) had a more concise result to the ultimate shear strength of SPD in the ex-

perimental test than the initial shear yield strength (IY) of the analytical approach. However, the ultimate shear strength occurred with a decreasing deformation magnitude as the loading angle increased. The specimens at angles 0° and 15° reached their ultimate shear strength with values at 0.17 rad and 0.13 rad drift angle, respectively. Meanwhile, the specimens with angles 30° and 45° achieved the ultimate shear strength at 0.02 rad drift angle. Even though the early buckling triggered the softening at small plastic deformation levels in all specimens, the specimens at 0° and 15° could restore the post-yield stiffness to be positive until reaching ultimate shear strength. In contrast, the specimens 30° and 45° continued to soften until reaching the maximum deformation of cyclic loading assignment.

3.1.4 Failure state

In the failure state investigation following Wang et al. (2021), the shear resistance of 85% of maximum strength was achieved at 0.15 rad to 0.22 rad drift angle, as shown in Figure 7. The average failure deformation was 0.19 rad and 0.18 rad for positive and negative load directions, respectively. The failure deformations and failure mechanism (FM) visualization can be seen in Figure 8.

Different loading angles resulted in different failure mechanisms. Failure in S-58.8-0° and S-58.8-15° due to diagonal web tension fracture in the middle zone (FM-1). A combination of failure mechanisms in the middle spot (FM-1) and corner web's edge-to-base plate welding interconnection (FM-2) occurred in specimens S-58.8-30°. In comparison, specimen S-58.8-45° occurred to fracture at the corner web's edge to base plate welding interconnection and web's edge welding intra-connection (FM-2 and FM-3).

3.1.5 Energy dissipation

On average, significant energy dissipation was achieved from 0.01 rad to 0.15 rad drift angle, as shown in Figure 9 (a). In better results, S-58.8-0° and S-58.8-30° specimens maintained energy dissipation up to 0.20 rad and 0.19 rad drift angles, respectively.

The S-58.8 specimens achieved 20% to 40% of the equivalent viscous damping ratio at 0.01 rad to 0.02 rad drift angle, as shown in Figure 9 (b). From 0.02 rad up to 0.15 rad, a stable equivalent viscous damping ratio with a magnitude range of 40% to 45% was preserved.

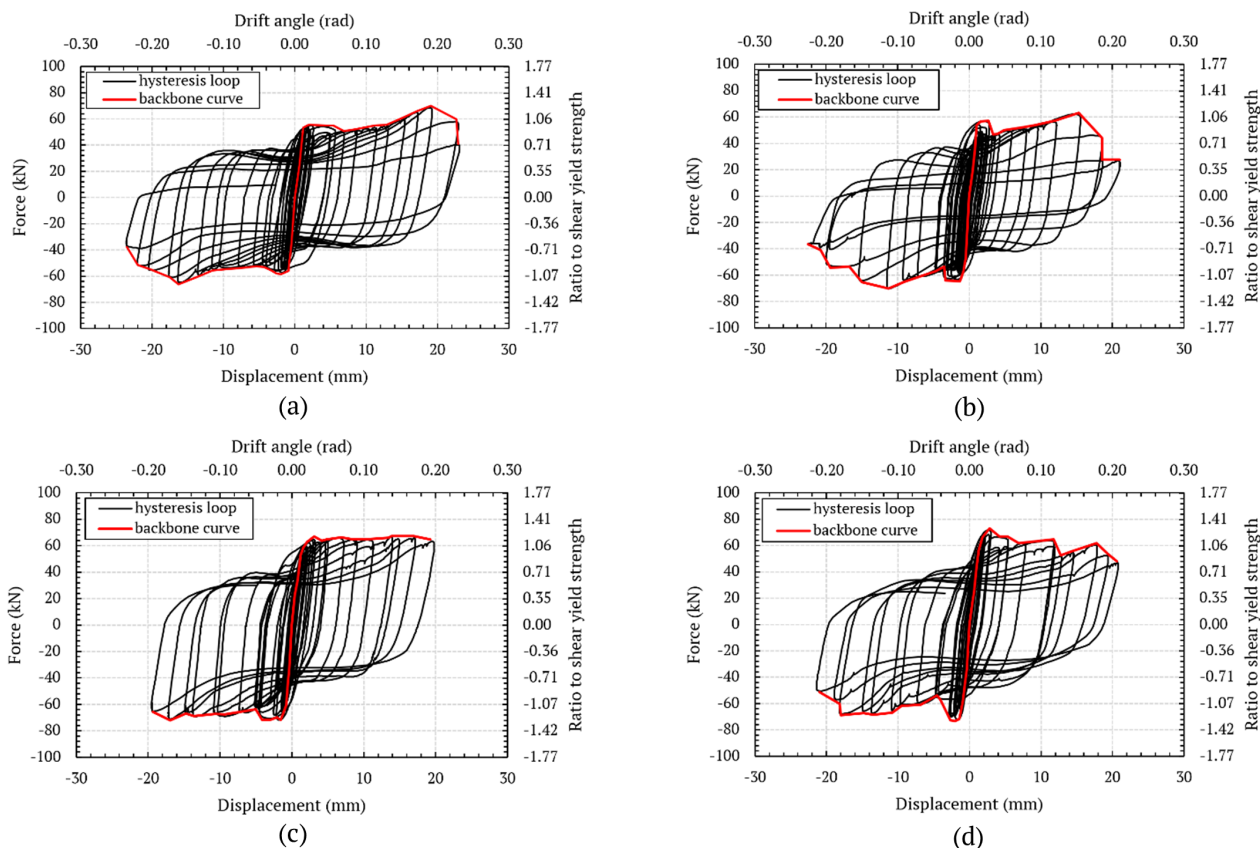


Figure 5 Hysteresis loop and backbone curve of the S-58.8 specimens under load angles: a) 0°, b) 15°, c) 30°, and d) 45°. *Note: the bottom and top horizontal-axis express the lateral displacement and drift angle (rotation) of MBSD, respectively; the left and right vertical-axis express the lateral force resistance and ratio lateral force resistance to the shear yield strength.



Figure 6 The deformed shape of the S-58.8 specimens in buckling state under load angles: a) 0°, b) 15°, c) 30°, and d) 45°.

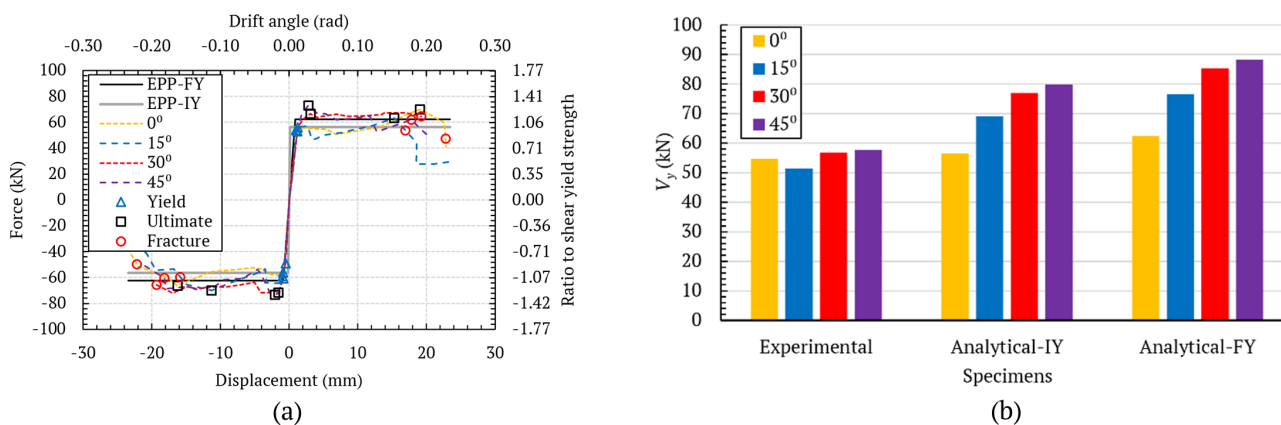


Figure 7 Shear strength of the specimens: (a) backbone curve S-58.8 specimens based on and (b) comparison of the shear yield strength of experimental to the analytical.

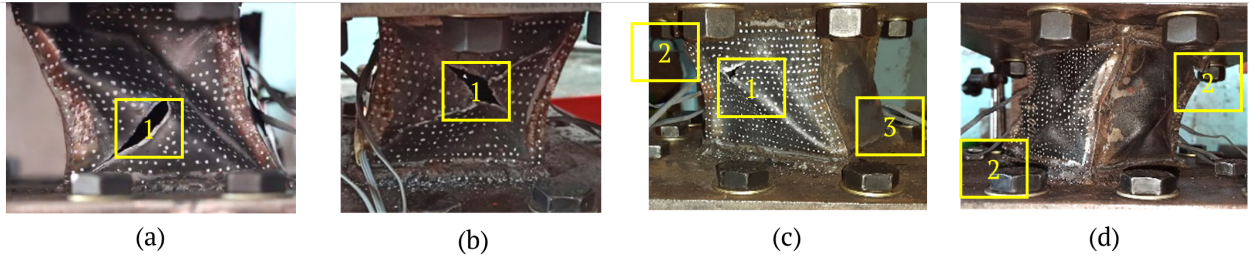


Figure 8 The deformed shape of the S-58.8 specimens with a thickness of 1.7 mm on failure state under load angles: a) 0°, b) 15°, c) 30°, and d) 45°. Noted*, 1 is "FM-1"; 2 is "FM-2"; and 3 is "FM-3".

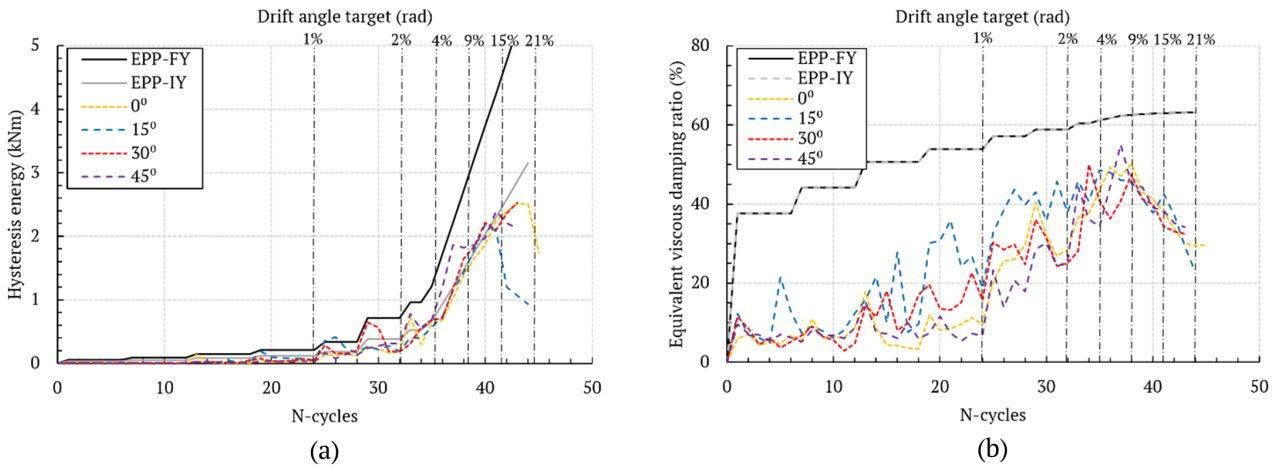


Figure 9 Energy dissipation achievement comparison of the S-58.8 specimens in each cycle: (a) energy dissipation and (b) equivalent viscous damping ratio.

3.2 S-27.0 specimens

3.2.1 Hysteresis loop

According to the experimental results, the stable hysteresis loop of the S-27.0 specimens was achieved in the 0.11 rad to 0.16 rad drift angles, as shown in Figure 10. The web buckling was not significant in these states, as shown in Figure 10 and Figure 11. Specimens S-27.0-0 and S-27.0-45° (with ultimate deformation capacity of 0.16 rad) showed longer stable hysteresis loops than the S-27.0-15° and S-27.0-30° (with ultimate deformation capacity of 0.11 and 0.14 rad, respectively).

3.2.2 Shear yield strength

The backbone curve and limit state for S-27.0 specimens are shown in Figure 12 (a) and (b). The shear yield strength of the S-27.0 specimens was in the range of 100 kN to 130 kN. In general, on the increment of the loading angle, the shear yield strengths of each specimen increased with a significant pattern, except the S-27.0-15° has a lower shear yield strength than S-27.0-0. In comparison, as shown in Figure 12 (b), even though the initial shear yield strength (IY) with analytical approach of specimen S-27.0-0° exhibited a coincident result to the experimental result, there was a slight

sharper increment trend as the larger the loading angle direction. In addition, the full shear yield strength (FY) of the analytical approach showed an equal trend with a larger magnitude than the initial shear yield strength (IY).

3.2.3 Ultimate state

Based on the experimental results, the average ultimate shear strength was 1.53 times greater than the shear yield strength, as shown in Figure 12. Thus, the ultimate strength to the yield strength ratio of the S-27.0 specimens was more significant than specimen S58.8. The loading angle effect also generated a more uniform drift angle capacity in the ultimate shear resistance. According to the analytical approach, as shown in Figure 12 (a), the full shear yield strength (FY) had a better similar result to the ultimate shear strength of SPD in the experimental test than the initial shear yield strength (IY) of the analytical approach. In addition, the experimental result showed a trend that the larger loading angle direction induced larger ultimate shear yield strength than the analytical result.

3.2.4 Failure state

According to the experimental backbone curve, the 85% after ultimate shear strength reached 0.14 rad to 0.22 rad drift angle, as shown in Figure 12. The average ultimate deformation was 0.19 rad and 0.17 rad for positive and negative load directions, respectively. In this state, the failure deformation visualizations and failure mechanism (FM) are shown in Figure 13.

3.2.5 Energy dissipation

Based on the experimental results, significant energy dissipation was achieved at around 0.03 rad drift angle, as shown in Figure 14 (a). The stable energy dissipation

was maintained in the range of 0.14 rad to 0.16 rad of the drift angle. Both specimens S-27.0-0° and S-27.0-15° could preserve the energy dissipation achievement until 0.15 rad of drift angle. In comparison, specimens S-27.0-30° and S-27.0-45° could maintain the energy dissipation until 0.14 rad and 0.16 rad of drift angles, respectively.

The S-27.0 specimens achieved 20% to 35% of the equivalent viscous damping ratio at a 0.03 rad to 0.09 rad drift angle, as shown in Figure 14 (b). Then, in the range of 0.09 rad up to 0.15 rad of drift angle, the stable equivalent viscous damping ratio with a magnitude range of 35% to 50% was preserved

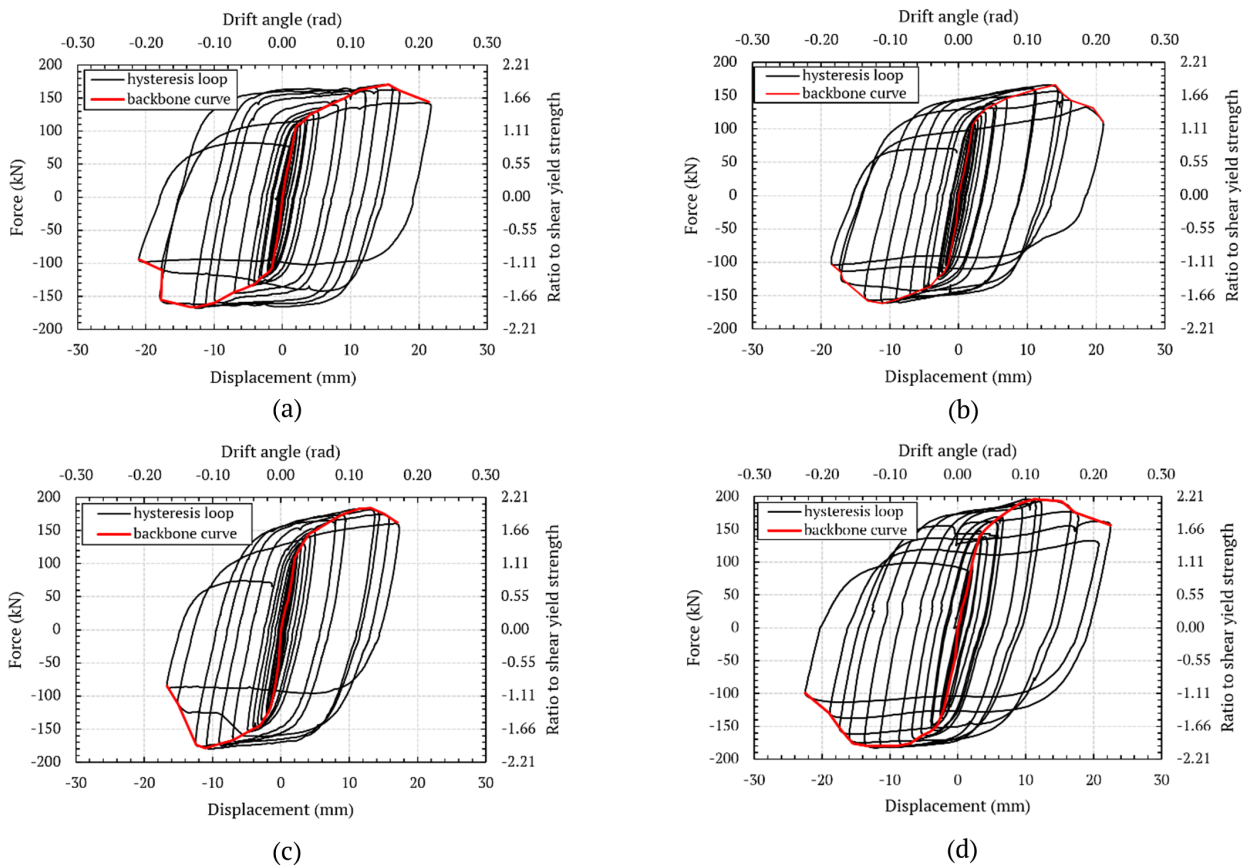


Figure 10 Hysteresis loop and backbone curve of the S-27.0 specimens under load angles: a) 0°, b) 15°, c) 30°, and d) 45°. *Note: the bottom and top horizontal axes express the lateral displacement and drift angle (rotation) of MBSD, respectively; the left and right vertical axes express the lateral force resistance and ratio lateral force resistance to the shear yield strength.

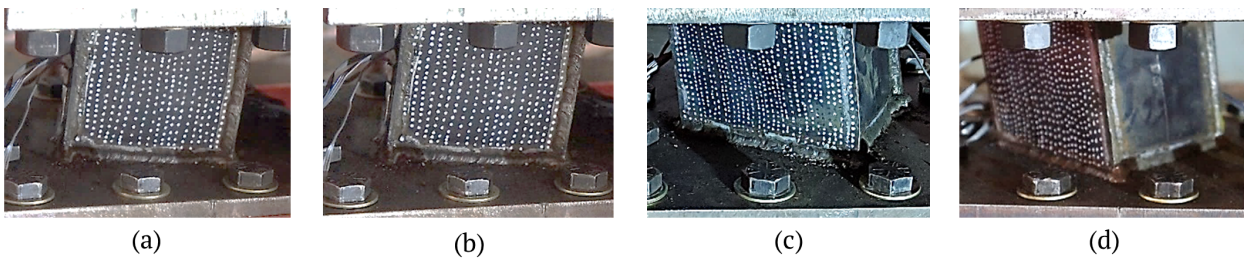


Figure 11 The deformed shape of the S-27.0 specimens in buckling state under load angles: a) 0°, b) 15°, c) 30°, and d) 45°.

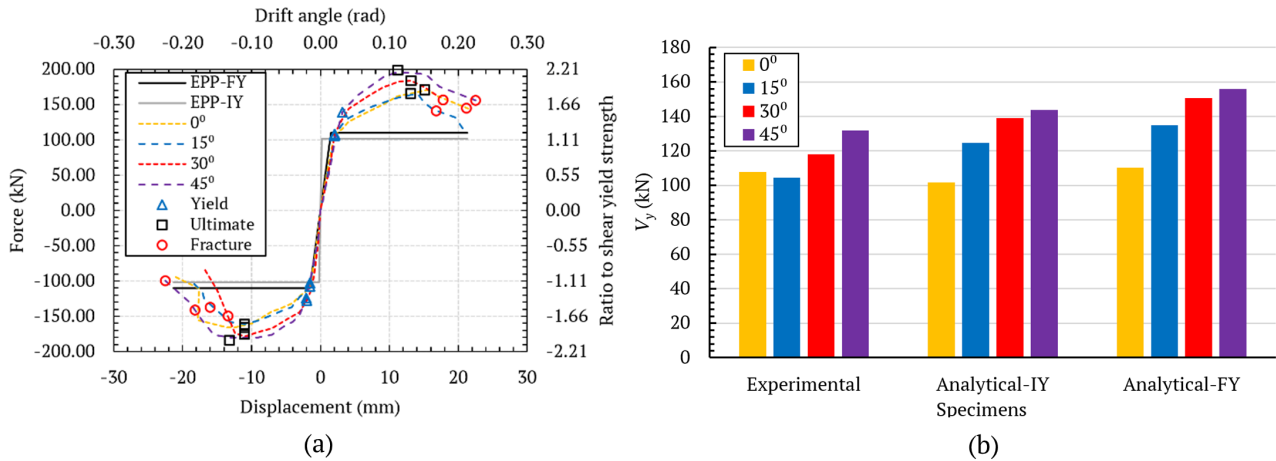


Figure 12 Shear strength of the specimens: (a) backbone curve S-27.0 specimens based on and (b) comparison of the shear yield strength of experimental to the analytical.

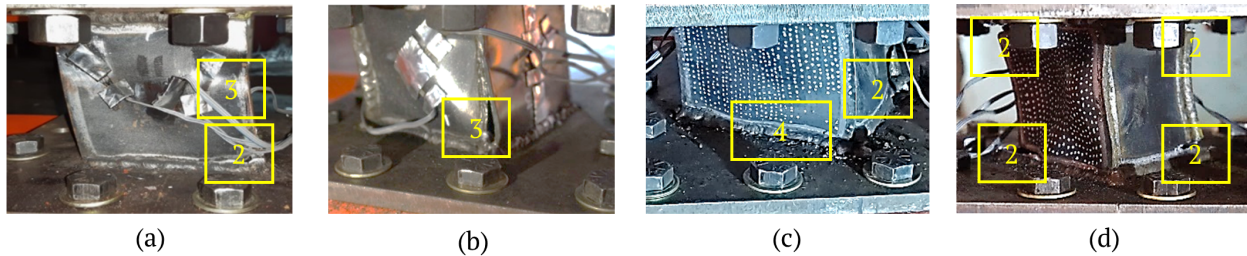


Figure 13 The deformed shape of the S-27.0 specimens with a thickness of 1.7 mm on failure state under load angles: a) 0°, b) 15°, c) 30°, and d) 45°. Noted*; 1 is "FM-1"; 2 is "FM-2"; 3 is "FM-3"; and 4 is "FM-4".

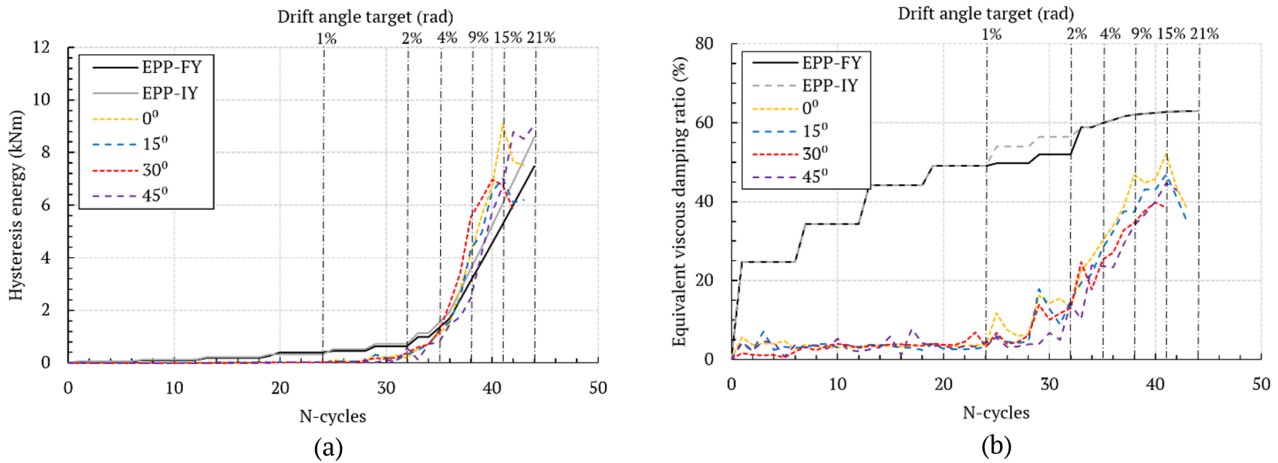


Figure 14 Energy dissipation achievement comparison of the S-27.0 specimens in each cycle: (a) energy dissipation and (b) equivalent viscous damping ratio.

4 DISCUSSION

4.1 Hysteresis loops

In discussing the hysteresis loop character of S-58.8 specimens, the premature plastic web buckling triggered the pinching under a 0.02 rad to 0.05 rad drift angle. The result was in line with the study by Chan et al. (2009) and Chen et al. (2013) which found that the slen-

der web of shearing damper exhibits more plastic buckling with slight pinching hysteresis loops. Even though web buckling started in early plastic deformation and continued to more significant displacement, as shown in Figure 6 and Figure 7, the shear resistance of specimens 58.8-0° and S-58.8-15° was maintained until 0.16 rad of the drift angle. However, after the plastic buckling occurred, the specimens S-58.8-30° and S-58.8-45° could not preserve the hysteresis loop stability, possi-

bly due to the loading direction causing relatively significant work out-of-plane of the shearing damper web.

The stable hysteresis loop of the S-27.0 specimens without web buckling at the 0.11 rad to 0.16 rad drift angle align with the study by Tanaka and Sasaki (2000), which found that a stocky web panel (slenderness less than 40) could achieve stable hysteresis energy performance. Thus, positive post-yield stiffness was formed from the yielding stage until the ultimate shear strength. After that, softening, which indicates strength degradation occurred. The shear resistance was preserved until 85% of ultimate shear strength with a 0.17 rad to 0.21 rad drift angle. In addition, the hysteresis loop of specimen S-27.0 was plumper than that of specimen S-58.8.

4.2 Shear yield strength

The shear yield strength of S-58.8 comparison between the experimental and analytical approaches is shown in Figure 7. It was found that the best estimation in quantifying the observed shear yield strength came from analytical approach, which considers the web's initial yielding (lower bound) in Equation (1). This aligns with the numerical modeling study by Awaludin et al. (2022) on the bi-directional box shear panel damper with a square hollow section. In addition, the increase of the shear yield strength of experimental results related to the loading angle increment was slower than the proposed analytical approach, as formulated in Equation (4). The early plastic buckling occurrence might have triggered this trend.

Regarding shear yield strength achievement of the S-27.0 specimens, it also aligned more closely with the lower bound shear yield formulation for the initial shear yield strength (IY) web part, as the Equation (1) as studied by Awaludin et al. (2022). Furthermore, the general trend, the shear yield strength increased with the increment of the loading angle of each specimen, as formulated in Equation (4), except for specimen S-27.0-15°. The S-27.0-15° generated a slightly smaller shear yield strength than S-27.0-0°. The S-27.0-15° specimen under a 15° loading angle, geometric imperfections from fabrication process might have inflicted more severe buckling in a significant out-of-plane load component. Thus, this reduced the shear yield strength.

4.3 Ultimate state

The ratio of ultimate shear strength to shear yield strength achievement for S-58.8 ranged of 1.1 to 1.6, which was in line with the previous study by Chen et al. (2013). However, a sharper loading angle might have triggered rupture at the corner of the web's edge where it connects to the to base plate via welding and each

web's edge of weld connection leading to premature strength degradation (FM-2 and FM-3), as shown in Figure 8. Thus, the S-58.5 specimens with loading angles 0° and 15° were proper for damper devices due to their sufficient stable shear resistance on significant plastic deformation. In contrast, the S-58.5 specimens with loading angles 30° and 45° were unsuitable for damper devices due to insufficient stable shear resistance during significant plastic deformation.

The ultimate shear strength for S-27.0 also ranged from 1.1 to 1.6 times the shier yield strength, coinciding with the study result from Chen et al. (2013). In addition, positive post-yield stiffness from yielding until ultimate shear strength was observed in all specimens. Generally, ultimate shear strength increased with greater loading angle, except for specimen S-27.0-0°, which achieved a larger shear strength than S-27.0-15°. Overall, ultimate shear strength specimens underwent deformation in the range of 0.11 rad and 0.13 rad of drift angle. A more consistent deformation pattern in ultimate shear resistance across varied loading angles was likely due to the stockier webs, which could withstand premature buckling formation.

However, higher shear resistance in stockier webs led to more severe stress concentration of the web's boundary connections, which could initiate the fracture, as shown in Figure 13. Hence, ultimate shear strength deformation was achieved relatively consistently before the fracture occurred. This unfractured deformation state could serve as a deformation limit design criterion for MBSD applications in bridge structures with the lowest performance limit.

4.4 Failure state

In all S-58.8 specimens, diagonal tension failure occurred due to diagonal tension except in S-58.8-45°. The slender web shape provoked the inelastic buckling formation. When inelastic buckling occurred, the shear lateral resistance was weakened, transferring lateral resistance to diagonal tension action. At larger cyclic displacement, the reversal of tension to compression increased diagonal tension strain, leading to diagonal tension fracture.

The majority failure state in specimen S-27.0 was triggered by the welding connection fracture, as shown in Figure 13. Failure due to diagonal web tension fracture in the middle zone (FM-1) did not occur in any S-27.0 specimens. Meanwhile, the majority of failure mechanisms were fractured corner web's edge to base plate welding interconnection (FM-2) for S-27.0-0°, S-27.0-30°, and S-27.0-45° specimens. For S-27.0-0° and S-27.0-30° specimens, this FM-2 failure was combined with the fracture of web's edge welding intra-connection (FM-3) and web's edge-to-base plate weld-

ing interconnection (FM-4), respectively. Furthermore, S-27.0-15° specimens only failed due to a fracture at the web's edge welding intra-connection (FM-3).

4.5 Energy dissipation

Compared to the elastic-perfectly plastic hysteretic energy models with initial yielding (EPP-IY) and fully yielding (EPP-FY) approaches, the S-58.8 specimen results were in intermediate, as shown in Figure 9. Up to a 0.14 drift angle, the energy dissipation increased with the loading angle. This likely corresponds to the shear strength due to the force vector from the web, as in the previous discussion about the shear yield and maximum shear strength. However, with increasing loading angles, the maximum deformation for stable energy dissipation decreased. The probable reason was that sharper loading angle produced a higher stress concentration, triggering the fracture mechanism following FM-2 and FM-3 at smaller deformation.

For S-27.0, significant energy dissipation was observed at 0.03 drift angle, as shown in Figure 14 (a). The stable energy dissipation could be maintained in the range of 0.14 rad to 0.16 rad of the drift angles. Both specimens S-27.0-0° and S-27.0-15° could preserve the energy dissipation achievement until 0.15 rad of drift angle. In comparison, specimens S-27.0-30° and S-27.0-45° could maintain the energy dissipation until 0.14 and 0.16 of drift angles, respectively. Compared to the elastic-perfectly plastic hysteresis energy with lower bound (using IY) and upper bound (using FY) approaches, the energy dissipation achievement of experimental results was beyond both. A highly probable reason for this is that the high over-strength ratio generated greater energy dissipation compared to the elastic-perfectly approach.

In terms of equivalent viscous damping ratio, a comparable range of achievement was also obtained by Zahrai (2015) for an ordinary SPD, which achieved a maximum equivalent viscous damping in the range of 35.5% to 40.2%. Xiao et al. (2022) also found that a shear square section steel tube damper reached 21% to 33% of an equivalent viscous damping ratio, which indicates that the MBSD proposed in this study could achieve a better result.

5 CONCLUSION

The experimental study and numerical analysis of the MBSD were performed under cyclic loading to investigate its structural behavior, i.e., hysteresis loop characteristics, shear yield strength, ultimate state, failure state, and energy dissipation. Hence, some notable results could be affirmed:

MBSD could achieve shear resistance with sufficient

energy dissipation across varied loading angles in the range from post-yield to ultimate deformation. The increment in the loading angle directions relative to one of the web planes increased both the shear yield strength and ultimate shear strength, except for the experimental results where the loading angle of 0° achieved a larger shear strength than the specimen with a loading angle of 15° in both the specimens of S-58.8 and S-27.0. The increment in loading angles also generated differences in terms of the ultimate state and fractured state. In addition, the average quantified equivalent viscous damping ratio under a 0.03 rad to 0.14 rad drift angle was in the range of 20% to 50%.

Generally, in both the S-58.8 and S-27.0 specimens, the shear yield strength achievement of the experimental results coincided with the upper bound analytical approach with an initial yield idealization of a web in an ordinary shear panel damper. The ultimate to-yield strength ratio characteristic of the experimental MBSD was still identical to that of an ordinary shearing damper with mild steel.

A stockier web generated more stable post-yield stiffness with minimized web buckling. However, it triggered slightly earlier strength degradation during plastic deformation due to the fracture of the intra-connection between each web and the interconnection of the web to the base plate.

The S-27.0 specimen had sufficient seismic performance under varied loading angles. Thus, it was viable for application in a bridge structure. The lowest performance achievement (unfractured state) of the S-27.0 specimens with a 0.11 rad drift angle on ultimate shear strength could be adopted for bridge structure seismic device design. Indeed, the compatibility of the proposed seismic device should comply with the lateral strength and deformation capacity of the bridge structural system.

For a future study, a numerical analysis using the finite element method needs to be conducted to investigate the stress and deformation mechanism of MBSD. Furthermore, the reliable application of MBSD in a bridge pier structure needs to be demonstrated by experimental and numerical studies. In addition, a larger ultimate elongation capacity of the steel material needs to be implemented to achieve a larger deformation capacity of MBSD.

DISCLAIMER

The authors declare that they have no known competing financial interests or personal relationships that could have influenced the work in this article.

ACKNOWLEDGMENTS

The authors would like to thank the Head of Materials Laboratory, Structural Laboratory, and Department of Civil and Environmental Engineering, Faculty of Engineering, Universitas Gadjah Mada, for supporting this study. The authors would also like to thank PT Wijaya Karya Beton Tbk., who supported the research and product development funding.

REFERENCES

- Abebe, D. Y., Kim, J. W., Gwak, G. and Choi, J. H. (2019), 'Low-cycled hysteresis characteristics of circular hollow steel damper subjected to inelastic behavior', *International Journal of Steel Structures* **19**(1), 157–167.
URL: <https://doi.org/10.1007/s13296-018-0097-8>
- AISC (2020), *Specifications for Structural Steel Buildings*, American Institute of Steel Construction.
URL: <https://doi.org/10.1061/taceat.0001170>
- AISC (2022), *Seismic Provisions for Structural Steel Buildings*, American Institute of Steel Construction.
- Awaludin, A., Setiawan, A. F., Satyarno, I. Shuanglan, W. and Haroki, Y. (2022), 'Finite element analysis of bi-directional shear panel damper with square hollow section under monotonic loading', *Journal of The Civil Engineering Forum* **8**(2), 157–168.
URL: <https://doi.org/10.22146/jcef.3842>
- Chan, R. W. K., Albermani, F. and Williams, M. S. (2009), 'Evaluation of yielding shear panel device for passive energy dissipation', *Journal of Constructional Steel Research* **65**(2), 260–268.
URL: <https://doi.org/10.1016/j.jcsr.2008.03.017>
- Chen, Z., Bian, G. and Huang, Y. (2013), 'Review on web buckling and hysteretic behavior of shear panel dampers', *Advanced Steel Construction* **9**(3), 205–217.
URL: <https://doi.org/10.18057/IJASC.2013.9.3.3>
- Chen, Z. Ge, H. and Usami, T. (2007), 'Study on seismic performance upgrading for steel bridge structures by introducing energy-dissipation members', *Journal of Structural Engineering* **53**, 540–549.
- Emilidardi, A. M., Awaludin, A., Triwiyono, A., Setiawan, A. F., Satyarno, I. and Santoso, A. K. (2024), 'Seismic performance enhancement of a pci-girder bridge pier with shear panel damper plus gap: Numerical simulation', *Earthquakes and Structures* **27**(1), 569–582.
URL: <https://doi.org/10.12989/eas.2024.27.1.569>
- Emilidardi, A. M., Setiawan, A. F., Awaludin, A., Satyarno, I. and Sunarso, M. (2022), Numerical model of finned tubular shear panel damper for multi-direction seismic excitation, in 'S. Belayutham, C.K.I.C. Ibrahim, A. Alisibramulisi, H. Mansor and M. Billah, eds. Proceedings of the 5th International Conference on Sustainable Civil Engineering Structures and Materials', pp. 751–766.
URL: <https://doi.org/10.1007/978-981-16-7924-7>
- Haroki, Y., Awaludin, A., Priyosulistyo, H., Setiawan, A. F. and Satyarno, I. (2023), 'Seismic performance comparison of simply supported hollow slab on pile group structure with different operational category and shear panel damper application', *Civil Engineering Dimension* **25**(1), 10–19.
URL: <https://doi.org/10.9744/ced.25.1.10-19>
- Jacobsen, L. S. (1930), 'Steady forced vibrations as influenced by damping', *ASME Transactions* **52**(1), 169–181.
- Kori Effendi, M. and Yulianto, H. (2023), 'Parametric study of the effect of diameter-to-thickness ratio against bending and shear load on the behavior of round hollow structural section beam', *Journal of the Civil Engineering Forum* **10**(1), 11–22.
URL: <https://doi.org/10.22146/jcef.7135>
- Kurdi, Budiono, B., Moestopo, M., Kusumastuti, D. and Muslih, M. R. (2017), 'Residual stress effect on link element of eccentrically braced frame', *Journal of Constructional Steel Research* **128**, 397–404.
URL: <https://doi.org/10.1016/j.jcsr.2016.09.006>
- Nakamura, R., Kanaji, H. and Kosaka, T. (2014), Development and design of new steel pipe integrated pier with shear link, in 'Hanshin Expressway Company Limited. Osaka.'
- Nakashima, M., Iwai, S., Iwata, M., Takeuchi, T., Konomi, S., Akazawa, T. and Saburi, K. (1994), 'Energy dissipation behaviour of shear panels made of low yield steel', *Earthquake Engineering & Structural Dynamics* **23**(12), 1299–1313.
URL: <https://doi.org/10.1002/eqe.4290231203>
- Santoso, A. K., Awaludin, A., Sulistyono, D., Setiawan, A. F., Sumartono, I. H. and Purnomo, S. (2024), 'Comparative study of the seismic performance between simply supported psc box girder bridge equipped with shear panel damper (spd) and lead rubber bearing (lrb)', *International Journal of Technology* **15**(5), 1–10.
URL: <https://doi.org/10.14716/ijtech.v15i5.5750>
- Shrinkam, M. R. and Razzaghi, J. (2020), 'Experimental and analytical investigation on the behavior of metallic box-shaped dampers (bsd)', *Structures* **23**, 766–778.
URL: <https://doi.org/10.1016/j.istruc.2019.12.018>
- Sun, J., Manzanarez, R. and Nader, M. (2004), 'Comsuspension cable design of the new san francisco-oakland bay bridge', *Journal of Bridge Engineering* **9**(1), 101–106.
URL: [https://doi.org/10.1061/\(asce\)1084-0702\(2004\)9:1\(101\)](https://doi.org/10.1061/(asce)1084-0702(2004)9:1(101))

Tanaka, K. and Sasaki, Y. (2000), Hysteretic performance of shear panel dampers of ultra low- yield-strength steel for seismic response control of buildings, in '12th WCEE, ed. 12th World Conference on Earthquake Engineering', pp. 1–8.

Tetsuhiko, A. (2011), 'Shear-panel type damper, bearing structure of bridge using the same, and the bridge adopting the bearing structure'.

Tetsuhiko, A., Yuuji, F. and Tatsumasa, T. (2010), 'Shear panel-type damper and bridge'.

Utama, B. N., Satyarno, I., Setiawan, A. F., Awaludin, A. and Aditama, G. M. (2022), Finite element analysis for developing multi-direction crossing web type shear panel damper, in 'S. Belayutham, C.K.I.C. Ibrahim, A. Alisibramulisi, H. Mansor and M. Billah, eds. Proceedings of the 5th International Conference on Sustainable Civil Engineering Structures and Materials', pp. 735–749.

URL: <https://doi.org/10.1007/978-981-16-7924-7>

Wang, W., Song, J., Wang, W., Ding, X. and Lu, Z. (2021),

'Experimental investigation of the seismic behavior of low-yield-point corrugated steel plate dampers', *Journal of Structural Engineering* **147**(2), 1–14.

URL: [https://doi.org/10.1061/\(ASCE\)ST.1943-541X.0002924](https://doi.org/10.1061/(ASCE)ST.1943-541X.0002924)

Xiang, N., Alam, M. S. and Li, J. (2019), 'Yielding steel dampers as restraining devices to control seismic sliding of laminated rubber bearings for highway bridges: Analytical and experimental study', *Journal of Bridge Engineering* **24**(11), 15.

URL: [https://doi.org/10.1061/\(asce\)be.1943-5592.0001487](https://doi.org/10.1061/(asce)be.1943-5592.0001487)

Xiao, L., Li, Y., Hui, C., Zhou, Z. and Deng, F. (2022), 'Experimental study on mechanical properties of shear square section steel tube dampers', *Metals* **12**(3), 418.

URL: <https://doi.org/10.3390/met12030418>

Zahrai, S. M. (2015), 'Cyclic testing of chevron braced steel frames with ipe shear panels', *Steel and Composite Structures* **19**(5), 1167–1184.

URL: <https://doi.org/10.12989/scs.2015.19.5.1167>

[This page is intentionally left blank]